HOT-GAS TESTS FOR DYNA-SOAR STRUCTURES AND

MATERIALS DEVELOPMENT

By E. L. Kaminsky and H. W. Klopfenstein
Boeing Airplane Company

INTRODUCTION

During Phase I of the Dyna-Soar study, a considerable number of hot-gas tests were performed for purposes of developing materials and full-scale structural components intended for application to the Dyna-Soar reentry glider. The tests on full-scale components were feasibility tests, not proof tests. Proof testing of the Dyna-Soar vehicle will take place during actual flight of the vehicle. Prior to actual flight, preliminary flight tests like those of Pilotless Aircraft Research Division (PARD, now Applied Materials and Physics Division) of NASA and the Hyper Environmental Test System (HETS) of BMD, USAF, are contemplated, but hot-gas tests in ground facilities will be used as aids in the final choice of materials and structural designs. Resorting to hot-gas tests means becoming involved in the problem of simulating, in a ground facility, the reentry environment. This discussion deals primarily with this simulation problem; that is, with the types of tests performed, the degree of simulation obtained, the limitations of the facilities, and the results of the tests. The present investigation is restricted to tests on full-scale components.

SYMBOLS

C_L lift coefficient

c_p specific heat at constant pressure, Btu/(lb)(^{O}F)

h heat-transfer coefficient, Btu/(sq ft)(sec)(^{O}F)

m mass, lb

$\dot{q}$ heat flux, Btu/(sq ft)(sec)

S   surface area, sq ft

T   temperature, $^{\circ}$F

T_{aw} adiabatic wall temperature, $^{\circ}$F

T_{w} wall temperature, $^{\circ}$F

t   time, sec

W   vehicle weight, lb

ϵ total normal emissivity

σ Stefan-Boltzmann constant, 0.4759×10^{-12} Btu/(sq ft)(sec)$(^{\circ}R)^{4}$

DISCUSSION AND RESULTS

Calibration Tests

The purpose of the hot-gas tests was to determine whether full-scale structural components fabricated from various materials could survive exposure to test conditions intended to simulate the vehicle flight environment. In order to illustrate the nature of this environment, the conditions encountered by the nose cap of the Dyna-Soar glider during a typical reentry are discussed herein.

The heat flux shown by the dotted line in figure 1 is anticipated for the environment at the stagnation point on the glider nose cap. The maximum value reached is 178 Btu/(sq ft)(sec), and the corresponding radiation-equilibrium temperature, based on an emissivity of 0.9, is 4,060° F. The stagnation point is subjected to high heat fluxes for relatively long periods of time. For example, the time of exposure to heat fluxes in excess of 170 Btu/(sq ft)(sec) is 12 minutes; in excess of 160 Btu/(sq ft)(sec), 17 minutes; and in excess of 150 Btu/(sq ft)(sec), 20 minutes. Maximum values of other flight parameters, such as stagnation-point pressure, total enthalpy of the stream, relative stream velocity, and stream mass-flow rate for the same reentry trajectory, are tabulated in the second column of table I. Complicating the problem is the presence of an oxidation and erosion environment.

No present ground test facility can duplicate all flight parameters simultaneously; consequently, the question arose concerning which parameters should be simulated. Since some of the structural components on the Dyna-Soar glider are radiation-cooled designs fabricated from

refractory metals, which oxidize catastrophically if protective coatings fail, and refractory nonmetals, which can fail due to thermal stresses, oxidation, or erosion, it was decided that the heat flux, maximum surface temperature of the component, amount of oxygen in the gas stream, and time of exposure to high temperature were the important parameters. The importance of the parameters for these structural components is in contrast with those for ablating components, for example, where stagnation enthalpy is the most important quantity. In order to eliminate scale effects, it was also decided that tests would be performed on full-scale components.

The next problem to be resolved concerned the kind of test facility to be used. The practical choices were ram jet, rocket exhaust, or plasma jet. Early tests were conducted using ram-jet facilities for both leading-edge and nose-cap tests; however, these facilities were incapable of producing the maximum design heat flux and stagnation temperature of the nose cap. Also, the combustion products of the fuel used did not provide simulation of gas chemistry. Rocket-motor facilities will simulate maximum design heat flux and temperature. These facilities operate at pressures considerably higher than flight values and have the same problem as ram jets with regard to gas chemistry. The gas-stabilized-arc plasma jet at Chicago Midway Laboratories (CML) of the University of Chicago was selected because it met all requirements except time of exposure and because the facility was available on a schedule demanded by the test program. The compromise adopted concerning time of exposure is illustrated by the solid line in figure 1 for the nose cap. A single exposure in this facility is limited to $2\frac{1}{2}$ minutes. Hence, the component being tested was first heated to $2,700^\circ$ F in a furnace, swung into the gas stream for $2\frac{1}{2}$ minutes, returned to the furnace for about 30 seconds while the cathode on the arc unit was being changed, and then swung back into the stream. This process was repeated until a total of four $2\frac{1}{2}$-minute exposures had been run. At the end of the second exposure, the anode was replaced. The simulation of flight environment conditions obtained in the CML facility is shown in table I. Stagnation pressure and mass flow are higher than the corresponding values for the vehicle, and enthalpy and stream velocity are lower. The gas used in the facility was nitrogen, but sufficient air was entrained to provide an ample supply of oxygen at the component. Stagnation-point heat flux and equilibrium temperature were simulated.

In calibrating the CML test facility, two specimens for each type of structural component were used: a high-temperature specimen and a low-temperature specimen. The high-temperature specimen for nose caps is shown in figure 2. The specimen was fabricated from AGR graphite, and slots and grooves were machined into it to reduce heat flow by conduction

from the stagnation-point region. The base diameter of the specimen was smaller than that of the actual cap, but the nose radius was full scale. The specimen location required for simulation of heat flux and radiation-equilibrium temperature was found by the following procedure: After being placed at a selected distance downstream from the orifice of the arc unit, the specimen was subjected to a $2\frac{1}{2}$-minute exposure in the plasma flow, and the arc unit was then turned off. At that instant, the heat flux being emitted from the stagnation point of the specimen was measured by a recording radiation pyrometer, which had been calibrated previously. Measurements of heat flux were made at sufficient specimen positions in the stream to establish where the design heat flux of 178 Btu/(sq ft)(sec) occurred. Assuming that the emissivity of the graphite specimen was 0.9, the radiation-equilibrium temperature of $4,060°$ F is computed from the formula

$$\dot{q} = \epsilon\sigma\left(T_w + 460\right)^4 \tag{1}$$

The calibration of the test setup with the high-temperature specimen does not make available a means for evaluating the effect of difference in emissivity of a component from the calibration specimen, nor does it provide a means for obtaining the heat flux at points other than the stagnation point.

A low-temperature copper specimen, shown in figure 3, was used in the second step of the calibration. Built into the specimen were copper calorimeters, each containing a thermocouple. The specimen was first located in the apparatus at the position occupied previously by the high-temperature specimen, and a Transite shield was placed between the specimen and the arc unit. The arc unit was turned on and brought to full operating condition, and the Transite shield was removed. The temperature-time history for the thermocouple in each calorimeter was then recorded, and the test continued until incipient melting of the specimen was detected. Since the specific heat and mass of the copper calorimeter were known, it was possible to compute the net heat flux delivered to the calorimeter from the equation

$$\dot{q}_{net} = c_p \frac{m}{S} \frac{dT}{dt} \tag{2}$$

Since

$$\dot{q}_{net} = h\left(T_{aw} - T_w\right) - \epsilon\sigma\left(T_w + 460\right)^4 \tag{3}$$

and since the emissivity of copper is well known, the convective heat flux, which is:

$$\dot{q} = h\left(T_{aw} - T_{w}\right) \tag{4}$$

can be computed.

For convenience, the slope of the temperature-time curve was evaluated at a temperature of 800° F. The use of a number of calorimeters made it possible to obtain the heat-flux distribution over the specimen.

From these tests performed on the calibration specimens, two points were obtained for the variation of heat flux with surface temperature at the stagnation point shown in figure 4.

If it is assumed that the dependence of the heat-transfer coefficient on the wall temperature is weak, the heat flux is a linear function of the wall temperature, and a straight line can be drawn connecting the two points mentioned previously. The line for the nose-cap calibration in the plasma jet is shown in figure 4, and for comparison a line is also plotted for the vehicle with the assumption that the heat flux is constant. Plots of equation (1) for various values of emissivity are also shown in this figure. The intersection of an emissivity curve with the calibration line represents the heat flux and radiation-equilibrium temperature for the emissivity selected. With these curves, it was possible to estimate the actual emissivity and temperature of a nose-cap material based on measured heat flux. First, the heat flux was measured by the radiation pyrometer. With this value as an ordinate in figure 4, a horizontal line was drawn to the calibration line, and the radiation-equilibrium temperature and emissivity determined. The intersection of the emissivity curve with the vehicle line represents what the heat flux and temperature would be in flight.

The comparison between computed heat-flux distribution and the distribution measured on the low-temperature specimen is shown in figure 5. The discrepancy is partly due to the variation of temperature through the cross section of the jet issuing from the arc unit.

Test Results

Tests were performed at Chicago Midway Laboratories on full-scale nose caps and leading edges and on small, insulated skin panels and antenna-cover materials. The nose caps were provided under subcontract from Chance Vought Aircraft, Incorporated. The nose caps were constructed of hemispherical segments of ATJ graphite. Additional thermal capability was provided in the tip through the use of zirconia rods. Incipient

melting of the nose cap and oxidation and erosion of the graphite adapter occurred, but the nose-cap specimen survived the test.

The following summary of 6-inch-diameter leading-edge components tested in the CML facility includes the test conditions and results:

1. A composite segment fabricated of phosphate-bonded chromia-alumina reinforced with molybdenum wire was tested under unknown environmental conditions since the radiation pyrometer was not connected during the test. A small, shallow crack formed in the component parallel to and about 2 inches from the stagnation line, but the component survived the test.

2. A flame-sprayed multilayer laminate of alumina and molybdenum was tested at a recorded heat flux of 34 Btu/(sq ft)(sec), and emissivity of 0.4, and a radiation-equilibrium temperature of 3,150° F. The component smoked badly in the preheat furnace and delaminated in the plasma jet.

3. A circumferentially and longitudinally stiffened, welded columbium shell protected by Chromalloy N-1 coating was tested at a recorded heat flux of 32 Btu/(sq ft)(sec), an emissivity of 0.37, and a radiation-equilibrium temperature of 3,200° F. The outer layer of the coating melted and flowed. Three small holes approximately 1/8 to 1/4 inch in diameter appeared near the stagnation line, possibly due to impact of graphite against the specimen when a piece of the anode broke off in the arc unit and moved downstream.

4. A circumferentially and longitudinally stiffened, welded 33-percent-tantalum—columbium shell protected by Chromalloy N-1 coating was tested at the same environmental conditions as those for the previous specimen. Again, the outer layer of the coating melted and flowed, but the intermediate layer remained intact, and the substrate was protected. The component passed the test.

5. A circumferentially and longitudinally stiffened, welded 0.5-percent-titanium—molybdenum shell protected by Chromalloy W-2 coating was tested at a measured heat flux of 43 Btu/(sq ft)(sec), an emissivity of 0.7, and a radiation-equilibrium temperature of 2,900° F. There was a slight glassy discoloration of the surface, but the component passed the test.

6. A circumferentially and longitudinally stiffened, riveted 0.5-percent titanium—molybdenum shell protected by Chromalloy W-2 coating was tested at the same environmental conditions as those for the previous specimen. The same glassy discoloration appeared, but the component passed the test.

For all of these leading-edge tests, the component was preheated to 2,300° F before exposure to the plasma jet.

In addition to the CML tests, preliminary evaluation tests were performed in a ram-jet exhaust by the Marquardt Aircraft Company on 4-inch-diameter leading edges. Two designs were tested: a longitudinally stiffened 0.5-percent-titanium—molybdenum shell protected by Chromalloy W-2 coating and a phosphate-bonded alumina component reinforced with molybdenum wire mesh. The components were not preheated for these tests. The component, at room temperature, was swung into the exhaust gases of the ram-jet burner, held there approximately 20 minutes, and then swung out and allowed to cool to room temperature. On the typical molybdenum specimen, the maximum temperature reached during the first two tests was 3,025° F, and the component was unaffected after several test runs with a cumulative test time of $43\frac{1}{2}$ minutes at 2,800° F or higher. During the first test on the alumina component, the maximum temperature reached slightly exceeded 3,000° F, and two hairline cracks appeared during the cooling cycle. In the second test, the maximum temperature was 3,150° F. A slight change in shape occurred in the hottest area. The maximum temperature reached during the third test was about 3,200° F. There were no additional cracks and no further shrinkage.

Tests on full-scale graphite nose sections and molybdenum skirts were conducted in the ram-jet facility at Chance Vought Aircraft, Incorporated. The graphite was siliconized ATJ with and without a further multilayer coating of molybdenum, zirconia, and alumina. Welded and riveted skirt designs were tested. The molybdenum was chromized and also protected by the multilayer coating. In general, the tests indicated unsatisfactory performance of both cap and skirt. It was not possible to reach a stagnation-point temperature of 4,000° F in the ram-jet facility. The multilayer coating failed at the stagnation point and flaked off in some regions of the skirt. Based on the results of these tests, the design of the nose was changed. The tip was subsequently constructed from zirconia rods inserted into a siliconized graphite nose as described previously for the CML tests. The coating on the molybdenum skirt was changed to Chromalloy W-2.

CONCLUSIONS

1. Through the use of a gas-stabilized-arc plasma jet, it is possible to simulate, on full-scale structural components, the most severe heating conditions encountered during reentry of a hypersonic glider, but because of the short operating time of the plasma jet, it was not possible to simulate uninterrupted time of exposure to heating.

2. The plasma jet appears to be the only ground test facility which can approximate the gas chemistry during heating. The ram jet and rocket exhaust cannot provide this simulation. Also, the ram-jet and rocket-exhaust facilities are limited to lower enthalpies than plasma jets.

3. The plasma-jet facilities provided partial correction for possible errors in predicting emissivity of test parts. Plasma-jet facilities with enthalpy equal to flight conditions can provide essentially complete correction for errors in emissivity prediction.

4. Although testing with a plasma jet is limited to relatively small components compared with radiant-heat-lamp testing, it has the following advantages:

(a) Radiant-heat facilities cannot simulate nose-cap temperatures.

(b) Heat flux rather than controlled temperature is applied by plasma jet.

(c) It is possible to simulate environmental parameters such as oxidation and erosion with a distributed airload in a plasma jet.

(d) It is possible to avoid off-design thermal gradients such as those which occur when part of a radiant-heat setup fails.

TABLE I

COMPARISON OF CML ENVIRONMENT
WITH VEHICLE NOSE ENVIRONMENT

	CML	VEHICLE
STAGNATION POINT PRESSURE, LB/FT^2	2,116	350
ENTHALPY OF STREAM, BTU/LB	2,300	10,000
STREAM VELOCITY, FT/SEC	2,500	24,000
HEAT FLUX (ϵ=0.9), BTU/FT^2 SEC	178	178
STREAM MASS FLOW RATE, LB/FT^2 SEC	164	0.432
STAGNATION POINT EQUILIBRIUM TEMPERATURE (ϵ=0.9), °F	4,060	4,060
CHEMICAL SPECIES OF BOUNDARY LAYER	N & AIR, PART. ATOMIC & IONIZED	AIR, PART. ATOMIC & IONIZED

PLASMA JET SIMULATION
OF VEHICLE STAGNATION
POINT HEAT FLUX VERSUS TIME
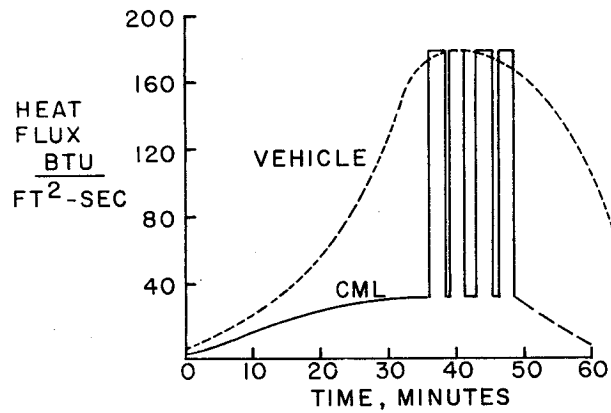
$$\frac{W}{SC_L} = 311 \quad \frac{LB}{FT}2$$

HEAT
FLUX
$\frac{BTU}{FT^2-SEC}$

200

160

120

80

40

VEHICLE

CML

0   10   20   30   40   50   60
TIME, MINUTES

Figure 1

CML HIGH-TEMPERATURE CALIBRATION MODEL
(NOSE CAP) AND INSTRUMENTATION

ARC UNIT

CALIBRATION MODEL
AGR GRAPHITE

FILTER

RADIATION
PYROMETER

PHOTOCELL

GALVANOMETER

EMF OF
PYROMETER

PYROMETER
CALIBRATION
CURVE
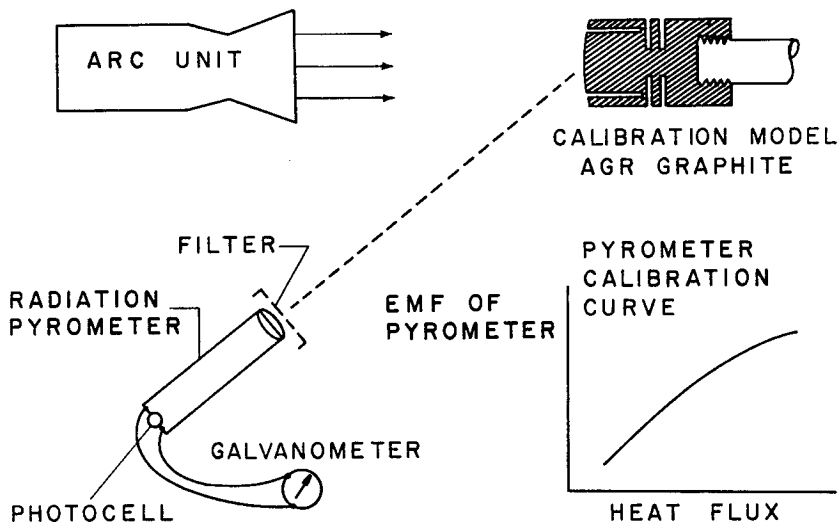
HEAT FLUX

Figure 2

CML LOW TEMPERATURE CALIBRATION MODEL
(NOSE CAP) AND INSTRUMENTATION

ARC UNIT

TRANSITE
SHIELD

COPPER
CALORIMETERS

COPPER
MODEL

TEMP.
800° F

$\dot{q}$, SLOPE

TIME

AMMETER
GALVANOMETER
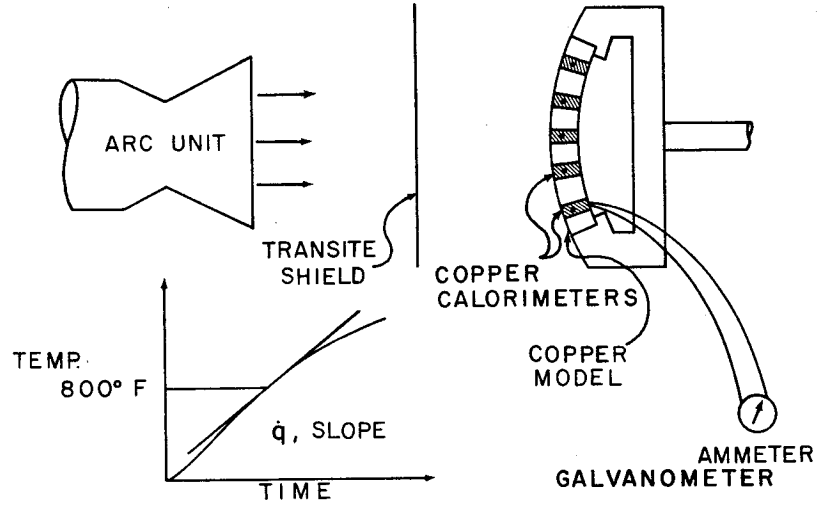
Figure 3

COMPARISON OF PLASMA JET AND VEHICLE
STAGNATION POINT HEAT FLUX

PLASMA JET

$\epsilon = 0.9$ $\epsilon = 0.7$

$\epsilon = 0.5$

VEHICLE

STING

MODEL NOSE CAP

ARC UNIT

200

150

100

50

HEAT FLUX
$\dfrac{BTU}{FT^2 - SEC}$
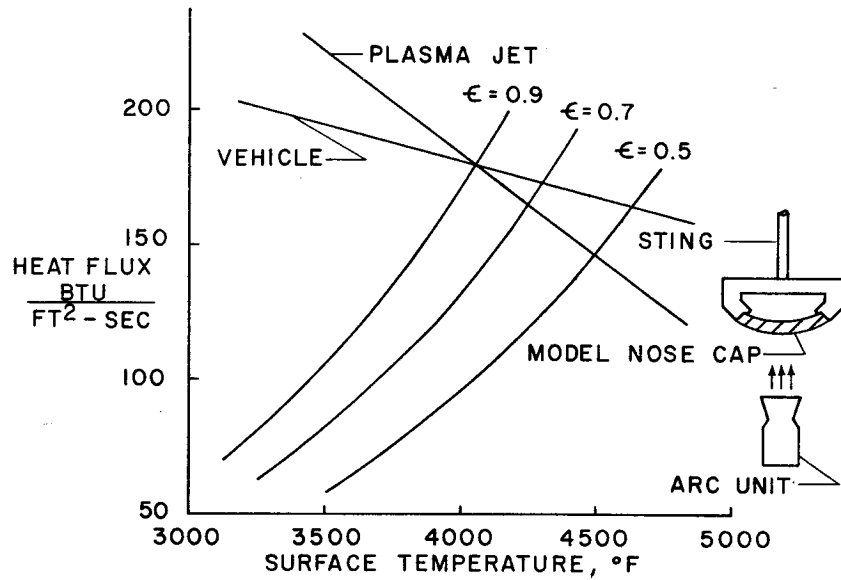
3000   3500   4000   4500   5000
SURFACE TEMPERATURE, °F

Figure 4

NOSE CAP HEAT FLUX DISTRIBUTION

Figure 5